Enhanced anti-fouling performance in MBRs using a novel cellulose nanofiber-coated membrane

Sarah Lotfikatouli[a], Pejman Hadi[b], Mengying Yang[b], Harold W. Walker[c], Benjamin S. Hsiao[b], Christopher Gobler[d, e], Michael Reichel[f] and Xinwei Mao[a,*]

[a] Department of Civil Engineering, Stony Brook University, Stony Brook, NY 11794

[b] Department of Chemistry, Stony Brook University, Stony Brook, NY 11794

[c] Department of Civil and Environmental Engineering, Worcester Polytechnic Institute, Worcester, MA 01609

[d] New York State Center for Clean Water Technology, Stony Brook University, Stony Brook, NY 11794

[e] School of Marine and Atmospheric Sciences, Stony Brook University, Stony Brook, NY 11794

[f] Town of Riverhead Sewer District, Riverhead, NY 11901

*Corresponding author:

Xinwei Mao

Address: 2429 Computer Science Building, Stony Brook University, Stony Brook, NY11794

e-mail: xinwei.mao@stonybrook.edu

Highlights

- The fouling of CNF-coated TFNC (TFNC-CNF) membranes is reversible.
- The TFNC-CNF membranes can enhance flux in submerged membrane bioreactors.
- TFNC-CNF membranes showed higher rejection of bio-foulants.
- Air scouring can enhance the flux of TFNC-CNF membranes when filtering wastewater.

Abbreviation List

ABS: Absolute

CAS: Conventional activated sludge

CNF: Cellulose nanofibrils

EPS: Extracellular polymeric substances

MBR: Membrane bioreactor

MLSS: Mixed liquor suspended solid

N: nitrogen

PAN: Polyacrylonitrile

PVDF: Polyvinylidene difluoride

SMBR: Submerged membrane bioreactor

SMP: Soluble microbial products

TC: Total carbohydrate

TEMPO: Tetramethyl-1-piperidinyloxy

TFNC: Thin-film nanofibrous composite

TMP: Transmembrane pressure

TOC: Total organic carbon

TP: Total protein

UW: Used and washed

WWTP: wastewater treatment plant

Graphical Abstract

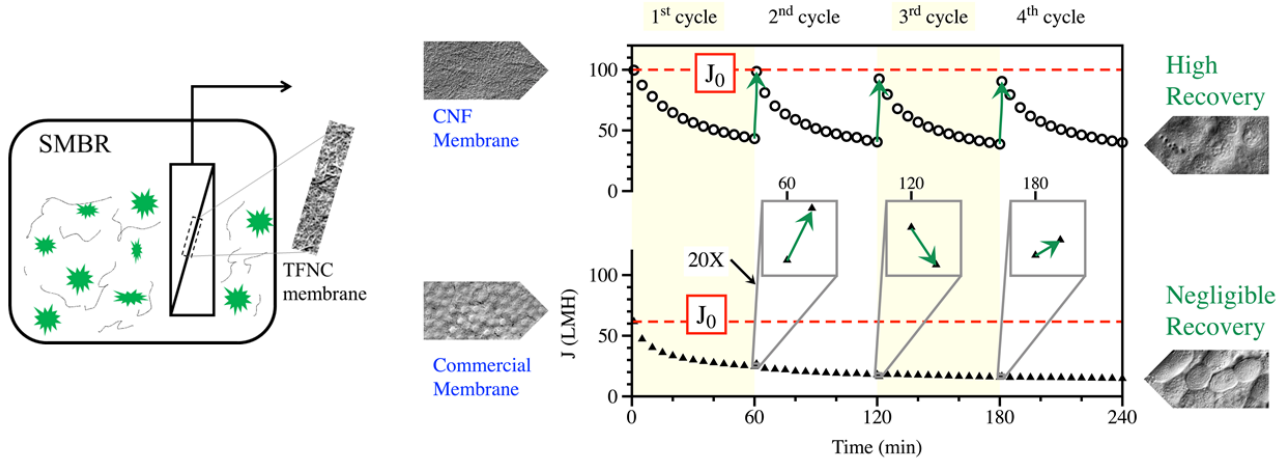

Abstract

A major challenge in using membrane bioreactors (MBRs) for wastewater nitrogen removal is membrane fouling. In this study, we compared the anti-fouling performance of a novel thin-film nanofibrous composite (TFNC) membrane with that of a conventional polyvinylidene fluoride (PVDF) membrane using real wastewater samples from an MBR municipal wastewater treatment facility. The demonstrated novel TFNC membrane consisted of a thin cellulose nanofiber (CNF) barrier layer coated on a nanofibrous non-woven substrate. Higher flux in the nanocellulose-coated TFNC membrane was observed compared with the PVDF membrane at all selected absolute transmembrane pressures (TMP_{abs}) (85.9 LMH vs. 45.1 LMH at $TMP_{abs=}$ 25kPa and 46.4 LMH vs. 21.4 LMH at TMP_{abs}= 55 kPa). The TFNC-CNF membrane also showed higher foulant rejection (>83.2% TOC rejection) than the PVDF membrane (<69.8% TOC rejection). The superior anti-fouling property of the TFNC-CNF membrane was primarily due to the super-hydrophilic nature and negative charge of the CNF surface layer. Specifically, the abundant carboxylate groups enhanced the negative surface charge on the TFNC membrane, confirmed by FTIR spectroscopy and zeta-potential measurements. The dead-end cell filtration test showed that the TFNC-CNF membrane recovered the initial flux by 98.9%, 92.8% and 90.7% after three consecutive mechanical cleaning processes; while the PVDF membrane's recovery rates were 43.3%, 26.7%, and 26.6%, respectively. Subsequent membrane filtration experiments with air scouring confirmed the superior anti-fouling characteristics of the TFNC-CNF membrane (59.2%, 80.4%, 76.6% and 86.8% % recovery) compared with the PVDF membrane (69%, 65.7%, 65% and 65.7% recovery) when filtering mixed liquor suspended solids (MLSS). Microscopic analysis also confirmed thinner cake layers formed on the TFNC-CNF membrane surface compared with the PVDF

membrane. The enhanced rejection rate and flux and more facile cleaning of TFNC-CNF membrane makes it a promising candidate for nitrogen removing MBRs.

Keywords: MBR, cellulose nanofiber, PVDF, thin-film nanofibrous composite, anti-fouling

1 Introduction

Industrial, municipal and agricultural wastewater is the major source of nitrogen pollution in waterbody, in the form of eutrophication and dissolved oxygen depletion (Rockström et al. 2009). Nitrogen compounds are usually removed from municipal wastewater streams in two interrelated steps of aerobic nitrification and anaerobic denitrification, which demand high energy consumption and large space, as well as yield excessive sludge (Bagchi et al. 2012, Jin and Zheng 2009). Membrane bioreactor (MBR) technology, with its superior performance over conventional activated sludge (CAS) treatment systems, has attracted a great deal of attention in the wastewater treatment industry (Judd 2010, Le-Clech 2010). MBRs consist of a bioreactor where biological processes take place followed by a membrane module for solid/liquid separation. Submerged membrane bioreactor (sMBR) is the main process configuration used in wastewater treatment, in which both microfiltration and ultrafiltration (MF and UF) are applied within the bioreactor to filter the treated effluent. MBRs offer a small footprint, high quality effluent, efficient removal of pathogens, and lower sludge yield (Judd 2006, Le-Clech 2010). Growth in the application of MBR, however, necessitates a substantial decrease in the membrane cost due to the fouling issue (Meng et al. 2009). For example, studies on cross-flow membrane modules in sMBRs often exhibit high degrees of fouling at the required high membrane flux or higher transmembrane pressure (He et al. 2005, Huang et al. 2011, Subtil et al. 2019).

MBR technology has been studied for biological nitrogen removal at various scales with the aim to reduce footprint and energy consumption in the last decade (Abbassi et al. 2014, Abegglen et al. 2009, Mao et al. 2020, Subtil et al. 2019). The majority of these studies involved the utilization of sMBRs in the main bioreactor or in an external tank (Falahati-Marvast and Karimi-Jashni 2020, Krzeminski et al. 2017). Although MBRs possess high potential for the removal of nitrogen from municipal wastewater, few studies have delved into the issues of membrane fouling in nitrogen removing MBRs (de Oliveira et al. 2018, Kraemer et al. 2012, Mao et al. 2020, Meng et al. 2009, Yang et al. 2009).

Membrane fouling during the filtration of wastewater occurs when membrane pores are obstructed by organics (proteins, polysaccharides etc.), inorganics or bio-related products or when a cake layer deposits on the surface of the membrane (Meng et al. 2009, van Reis and Zydney 2007). Factors that affect membrane fouling include feed wastewater characteristics, membrane properties (geometry, configuration, surface area and surface characteristics such as hydrophobicity) and operational conditions (Gander et al., 2000). Major contributors to membrane fouling in membrane bioreactors include soluble microbial products (SMP) and extracellular polymeric substances (EPS), which comprised of organic compounds such as substrate utilization-associated products (UAP) and biomass-associated products (BAP) (Laspidou and Rittmann 2002). EPS induces stabilization of cells and facilitates bio-floc aggregation. SMP and EPS consist of humic substances, proteins, DNA, lipids, polysaccharides, carbohydrates and other small molecules (Meng et al. 2009, Shi et al. 2017). SMP and EPS are generally not significant in the wastewater feed. Instead, the quantity and nature of SMP and EPS in MBRs depends on the feed characteristics (type and strength), environmental conditions (pH and toxicant presence), reactor

type, and operational parameters such as HRT and shock loads (Kunacheva and Stuckey 2014, Le-Clech et al. 2006, Mutamim et al. 2013).

In nitrogen removing MBRs, the effectiveness of the treatment process depends on a number of factors such as hydraulic retention time (HRT), dissolved oxygen (DO), and food to microorganism ratio (F:M). In wastewater treatment, higher oxygen levels result in improved sludge filterability and lower fouling. In nitrogen removing systems, however, lower levels of oxygen are generally required. A study by Arabi and Nakhla demonstrated increased SMP and EPS content in the MLSS at low DO levels (1.0-1.2 $mg.L^{-1}$), which negatively influenced fouling in comparison to higher DO levels (3.0-4.0 $mg.L^{-1}$) (Arabi and Nakhla 2009). There is conflicting data on how DO level influences EPS content of the bioreactor, i.e., a decrease in SMP was observed with decreasing DO from 3.4 to 0.9 $mg.L^{-1}$(Ji and Zhou 2006). While in other studies an increase in DO (0.8 to 2.1$mg.L^{-1}$) led to a decrease in protein (6.3 to 2.6 $mg.g^{-1}$MLSS) and carbohydrate (1.8 to 1.6 $mg.g^{-1}$MLSS) in SMP whilst protein content of EPS decreased (2.2 to 1.2 $mg.g^{-1}$MLSS) and carbohydrate content increased slightly (7.3 to 8.8 $mg.g^{-1}$MLSS) (Subtil et al. 2019).

Hydrophobic interactions between foulants and the membrane surface are particularly important in understanding and controlling fouling in MBRs (Yang et al. 2012). To reduce membrane fouling due to SMP and EPS in wastewater, varying techniques have been employed, including, but not limited to, membrane modification to engineer a more hydrophilic membrane surface (Hadi et al. 2019). To this end, membrane surface modification to enhance hydrophilicity have been achieved by various approaches: (i) chemical grafting of a zwitterionic polymer on the UF polyethersulfone (PES) membrane surface (Galiano et al. 2018) and of a hyperbranched polyglycerol (hPG) on the thin-film composite polyamide (PA) membrane surface (Liu et al.

145 2017), (ii) coating of titanium dioxide (TiO_2) and polydopamine (PDA) (Su et al. 2012), as well
146 as graphene (Gr)/polypyrrole (Ppy), graphene oxide (GO)/Ppy (Liu et al. 2013) and polyamide
147 graphene oxide (PA-GO) (Jin et al. 2018) on the surface varying membranes.

148 Cellulose is a abundant and sustainable biopolymer, possessing advantages such as water
149 stability, chemical resistance, high Young's modulus, and surface functionalization etc.
150 Nanocellulose fibers can be extracted from any lignocellulosic resources such as wood, non-wood
151 plants and microorganisms, using physical and chemical techniques. These nanomaterials are
152 ideally suited for contaminant removal from water through adsorption or membrane filtration
153 (Abouzeid et al. 2019, Ma et al. 2014). Membranes with cellulose nanofiber (CNF) coatings have
154 been studied for their anti-fouling potential with selected model molecules due to the abundant
155 hydroxyl and carboxyl functional groups on CNF introduced onto the membrane surface (Hadi et
156 al. 2019). High negative surface charge (due to the carboxylate groups at the appropriate pH level)
157 and hydrophilic properties of CNF-coated membranes are key features contributing to anti-fouling
158 behavior when interacting with model proteins (i.e. bovine serum albumin (BSA) (Hadi et al.
159 2019). CNF-coated membranes have been further evaluated in the water reclamation industry due
160 to its easy functionalizability for grafting anionic and cationic surface groups (Abouzeid et al.
161 2019) on the membrane surface. However, there has been no studies using CNF-coated membranes
162 for wastewater treatment.

163 In this study, we evaluated a thin-film nanofibrous composite-cellulose nanofiber (TFNC-
164 CNF) coated membrane to filter real wastewater collected from a nitrogen removing MBR and
165 compared the membrane fouling properties with those of commercially available polyvinylidene
166 fluoride (PVDF) membranes. We hypothesize that the fouling caused by interaction of functional
167 groups (carboxyl and hydroxyl) with EPS/SMP on the surface of the TFNC-CNF membrane is

significantly less compared with that of PVDF membranes. In addition, we further hypothesize that the mechanical strength of the TFNC-CNF membrane can withstand mechanical (i.e. air scouring) cleaning cycles. To test these hypotheses, a set of experiments were conducted to characterize the fouling behavior and flux recovery during ultrafiltration of (1) mixed liquor suspended solids (MLSS), and (2) the supernatant of the settling sludge (sludge-free) using TFNC-CNF and PVDF membranes. Fouled membranes and the permeate were analyzed to compare the extent of fouling for the different membrane materials. Findings of this study expand our knowledge of employing TFNC-CNF membranes for water reclamation and wastewater treatments, knowledge that can potentially inspire anti-fouling strategies in nitrogen removing MBRs.

2 Material and Methods

2.1 Materials

A commercial grade ultrafiltration membrane (UF): PVDF-A6 (MWCO 500 kDa) was selected as a reference in the fouling tests (Sterlitech). Chemicals used in the experiments included: analytical grade hydrochloric acid (HCl), potassium chloride (KCl), polyamide epichlorohydrin resin (PAE), formaldehyde (CH_2O), phenol (C_6H_5OH), sodium hydroxide (NaOH), polystyrene microspheres (0.05 μm and 0.1 μm) (Polysciences Inc.), total carbohydrate assay: BioLab kit (Fisher Scientific), and total protein assay kit (Sigma Aldrich).

189 **2.2 CNF Preparation**

190 Cellulose nanofibers extracted from bamboo pulp (carboxyl content=1.14 mmol/g) were
191 treated by the tetramethyl-1-piperidinyloxy (TEMPO) mediated oxidation method and the
192 resulting CNF suspensions were used for membrane fabrication (Ma et al. 2014). In brief,
193 electrospun nanofibrous substrate was soaked in the 0.1 wt % polyamide epichlorohydrin (PAE)
194 solution and hydrochloric acid (HCl 0.01 N) at the pH value of 1.9-2 until the pores were filled
195 with acidic solution (~5 min). Then the soaked electrospun nanofibrous substrate was placed on a
196 glass plate and the excess acidic solution was removed by rolling a glass rod on its surface.
197 Subsequently, 20 mL of CNF suspension (0.1 wt %) was poured on the surface of the electrospun
198 nanofibrous substrate, where a viscous gel layer was formed. The glass plate was then placed in
199 the oven and the TFNC-CNF membrane was baked at 110°C for 25 minutes or until the membrane
200 sheet started to dry from the edges. The casted TFNC-CNF membrane was then used for the
201 following experiments.

202 The pore sizes of both membranes were determined using filtration of polystyrene
203 microspheres in combination with the total organic carbon (TOC) rejection rate measurements
204 (Faccini et al. 2015). The nominal pore size analysis method is discussed in the Supporting
205 Information.

206

207 **2.3 MBR Experimental Setup**

208 A rectangular reactor with working volume of 40 L was used to hold the submerged flat sheet
209 membrane module (Figure 1 (A)). The membrane module had an effective surface area of 0.05
210 m^2 and was placed in the reactor with the option of additional air scouring. The diagram of the

overall system and a photo of the laboratory system are provided in the Supporting Information (Figures S1 and S2).

At stage 1, the reactor was operated at two constant transmembrane pressures (TMP_{abs}): 55 kPa and 25 kPa, using a vacuum pump. One filtration cycle (300 minutes) was conducted at each pressure to compare the fouling performance between the TFNC-CNF and PVDF membranes. To test each membrane, the reactor was filled with MLSS obtained from a nitrogen removing MBR at the Riverhead Wastewater Treatment Plant, in Riverhead, NY. The transmembrane pressure was monitored in the feed stream using pressure gauges and a digital balance was used to record the cumulative volume of permeate per minute. The volume of permeate was used to calculate the flux every five minutes using Equation 1 and the normalized flux (J_n) was calculated based on Equation 2.

$$J = \frac{V}{A.t} \qquad \text{Equation 1}$$

$$J_n = \frac{J}{J_0} \times 100 \qquad \text{Equation 2,}$$

where J is the flux (L m^{-2} h^{-1}, LMH), V is the volume of the permeate (L), A is the effective membrane surface area (m^2), t is the filtration time (h) and J_0 is the initial flux (L m^{-2} h^{-1}, LMH).

At stage 2 of the study, a Sterlitech stirred dead-end cell (HP 4750) filtration unit with working volume of 0.25 L was used for MLSS and supernatant filtration (Figure 1 (B)). Membranes were cut into circular disks with 4.3 cm diameter and each sample disk was placed on the porous support in the dead-end cell filtration setup. Four consecutive filtration cycles (each 60 minutes in duration) were conducted, each followed by a mechanical washing step with constant tap water flow at the membrane surface for 10 seconds. At the beginning of the dead-end cell filtration, distilled water was introduced for 30 minutes to complete the membrane compaction and obtain the steady state

flux. After that, the sludge or supernatant filtration was tested at 55 kPa (TMP_{abs}) (Fu et al. 2017). In order to prepare the sludge-free samples, the MLSS was centrifuged at 5000 rpm at 20 °C for 5 minutes and the supernatant was taken as the feed for membrane filtration. The MLSS and sludge free samples were used to investigate (i) the flux recovery after washing the used membranes and (ii) feed composition influence on membrane filtration performance.

At stage 3, an air scouring unit was added to the rectangular reactor in stage 1. The air scouring unit was connected to an air pump, which supplied continuous coarse air bubbles to the surface of the membrane at the rate of 10 LPM throughout the duration of the experiment. The reactor was operated at a constant TMP_{abs} of 55 kPa using a vacuum pump. Five consecutive filtration cycles (60 minutes/cycle) were conducted, each followed by a washing step as described in stage 2. Liquid samples of feed MLSS (50 mL) and permeate (15 mL) samples were collected for TOC, total protein (TP) and total carbohydrate (TC) measurement. Feed sample was collected at the start of the experiment and permeate samples were collected every 10 minutes for the first 60 minutes and hourly afterwards.

2.4 Membrane Characterization

The surface topography, morphology and cross section of the membranes were characterized by a focused ion beam scanning electron microscopy (FIB-SEM, crossbeam 340; Carl Zeiss Microscopy, LLC). Membrane samples were sputtered with Ag/Pd and were coated (10 nm thickness) at a high vacuum of 10^{-5} mbar (Leica EM ACE600). The surface functional groups of the pristine and used TFNC-CNF and PVDF membranes at different stages were characterized by Fourier transform infrared spectroscopy (FTIR, PerkinElmer Spectrum One) equipped with attenuated total reflection (ATR) configuration. The spectra with a resolution of 4 cm^{-1} and 64

scans per spectrum were recorded in the transmittance mode between the wave number range of 4000-400 cm^{-1}. Dynamic water contact angle of the membrane surface samples was analyzed by Dataphysics Contact Angle Analyzer (OCA 15 EC). In this test, 4 μL water droplets were generated using a syringe with a 0.52 mm inner diameter needle (ID) at a dosing rate of 2 μL/s. To measure the zeta potential (ζ) of the membrane surface, an Electrokinetic Analyzer was employed to measure the streaming potential of the membrane surfaces mounted on an adjustable gap cell (20 mm × 10 mm, gap distance = 110-120 μm) equipped the pH titration probe, where the pH value was varied from 4.5 to 8 using the 1 mM KCl electrolyte solution. The nominal pore size analysis of the two tested membranes was conducted using polystyrene microspheres, a detailed analysis is summarized in the Supporting Information.

2.5 Foulants Characterization

At stage 3, SMP samples were filtered through 0.45 μm filters and were stored at 4 °C before further analysis. EPS was chemically extracted from 10 mL sludge samples (collected at the start of experiment) using formaldehyde and sodium hydroxide (1 N) from feed sludge sample at 4 °C for 3 h, residual extractant in the suspension was removed by dialysis membrane filtration according to the procedures in the literature (Liu and Fang 2002). Liquid samples of feed wastewater (50 mL) and permeate (15 mL) liquid samples were harvested for TOC, TP and TC measurements: TOC was carried out using a Shimadzu TOC/TN analyzer, TP was conducted using the modified Lowry method (Peterson's modification) (Peterson 1977), TC was measured using the sulfuric acid-phenol method (Masuko et al. 2005).

3 Results

3.1 Membrane Fouling Comparison in Submerged Filtration Unit

In stage 1 experiments, two absolute transmembrane pressures (TMP_{abs}) (55 and 25 kPa) were selected to test the fouling performance of tTFNC-CNF and PVDF membranes in the submerged membrane filtration unit. The pressures selected in this study were based on the commonly used TMPs for MBRs treating domestic wastewater (Le-Clech et al. 2006). The PVDF-A6 membrane was chosen for comparison in this study since it exhibited similar flux and rejection rate of protein bovine serum albumin (BSA) as the TFNC-CNF membrane (Hadi et al. 2019). Both membranes had a mean pore size of 50 nm or less based on nominal pore size analysis (Supporting Information). The flux change of PVDF and TFNC-CNF membranes were monitored over 300 minutes at the defined pressure using 2950 ± 50 mg/L mixed liquor suspended solid (MLSS) (Figures 2(A) and 2(B)). The initial flux for TFNC-CNF membranes (85.9 LMH at 25 kPa and 46.4 LMH at 55 kPa) were found to be about twice of those for PVDF membranes (45.2 LMH at 25 kPa and 21.4 LMH at 55 kPa). During the filtration period, both membranes encountered abrupt fouling during the first 20 minutes operation with more than 25% of flux reduction as fouling developed and gradually started plateauing after 60 minutes. At the end of the experiment at 55 kPa TMP_{abs}, 19.4% of the initial flux was observed in the TFNC-CNF membrane, while the PVDF membrane had 32.3% of the initial flux. However, the flux in TFNC-CNF membrane (15.0 LMH) was much higher than that in the PVDF membrane (9.1 LMH). At the end of the experiment with 25 kPa TMP_{abs}, the flux in TFNC-CNF membrane (16.7 LMH) was comparable to that in the PVDF membrane (14.6 LMH).

300 **3.2 Membrane Flux Change and Recovery at Different Test Conditions**

301 At stage 2, a stirred dead-end cell filtration apparatus (Figure 1 B) was used to more
302 specifically investigate the interactions between bio-foulants and the membrane surfaces. Two
303 suspensions were filtered in these experiments: In one set of experiments, the MLSS were filtered
304 directly by both the TFNC-CNF and PVDF membranes (Figure 3, Panel A); in the second set of
305 experiments, only the supernatant of the centrifuged MLSS was used (Figure 3, Panel B). In the
306 experiments using MLSS, both SMP and EPS were present. In the experiments with sludge
307 supernatant, only SMP was present as most of the EPS was removed by the centrifugation process.
308 Based on results obtained from stage 1, an absolute TMP of 55 kPa was selected for the dead-end
309 filtration tests.

310 During stage 2, in the tests with MLSS, the initial flux of TFNC-CNF membrane was 99.7
311 LMH and the initial flux of PVDF membrane was 61.6 LMH. Both membranes were washed every
312 60 min. After each cycle of filtration of MLSS, the flux of the TFNC-CNF membrane decreased
313 to below 60% of the initial flux (56.6%, 59%, 58.1% and 56.1% of the initial flux for each
314 consecutive cycle) (Figure 3A). After each mechanical washing, the TFNC-CNF membrane was
315 able to recover more than 90% of the initial flux. The PVDF membrane flux decreased to 60.1%,
316 32.83%, 3.8% and 10% of the initial flux, respectively, at the end of each filtration cycle. After
317 mechanical washing very little flux recovery was observed for the PVDF membrane, and the
318 membrane underwent continuous flux declined with each filtration cycle (Figure 3A).

319 A similar trend of flux decrease and recovery was observed for the TFNC-CNF and PVDF
320 membranes in the sludge supernatant filtration tests (Figure 3B). In the supernatant filtration tests,
321 the initial flux of TFNC-CNF membrane was 111 LMH, and the initial flux of PVDF membrane
322 was 102.7 LMH. At the end of each filtration cycle, the flux of TFNC-CNF membrane decreased

to 51.1%, 46.4%, 41.2% and 39.9% of the initial flux, while the PVDF membrane flux decreased to 59.3%, 24.2%, 5.4% and 4.5% of the initial flux, respectively. Flux recovery after mechanical washing showed more reversible fouling for the TFNC-CNF membrane (94.8%, 83.7% and 82.2% recovery of the initial flux was recovered after each cycle) in comparison to PVDF membrane (only 40.7%, 28.5% and 23.8% recovery of the initial flux was observed for each cycle). Figure S3 illustrates the total permeate collected throughout the experiments and illustrates higher total permeate volumes for TFNC-CNF membrane compared with PVDF membranes. Furthermore, higher total permeate volume was collected during supernatant filtration compared with MLSS filtration.

When we compare the membrane fouling at the two test conditions: flux change and recovery, the TFNC-CNF membrane showed better flux recovery in case of MLSS filtration. However, considering higher initial flux (start of experiment) and final flux (at the end of the first cycle), it also indicates the improved filtration behavior of the TFNC-CNF membrane for supernatant filtration. In terms of initial flux after first wash for both conditions, average flux for MLSS and supernatant filtrations were 96.4 ±7.7 and 93.8 ± 4.3 LMH and are not considerably different while average final flux (after each cycle) were 39.7 ± 0.9 and 55.2 ± 1 LMH, respectively. In case of the PVDF membranes, the flux change trend was similar for the MLSS and supernatant filtration, and the membrane underwent continuous flux decline while at each time the flux for supernatant filtration was higher than for MLSS filtration.

3.3 Membrane Performance in Submerged Filtration Unit with Air Scouring

With the high flux and prominent flux recovery of the TFNC-CNF membrane observed in the dead-end cell filtration unit, we further explored membrane fouling and cleaning in the main

346 bioreactor with an air scouring module. At this stage, the TFNC-CNF membrane and the PVDF
347 membrane were operated in the same conditions as described in stage 1 (i.e., at 55 kPa TMP_{abs})
348 with the addition of continuous air scour. The initial fluxes for the TFNC-CNF and PVDF
349 membranes were 62.5 and 30.2 LMH, respectively. The TFNC-CNF membrane exhibited high
350 flux recovery of 59.2%, 80.4%, 76.6% and 86.8% of the initial flux after each cycle with
351 mechanical cleaning and continuous air scouring, while PVDF membrane flux recovery was 69%,
352 65.7%, 65% and 65.7%, respectively for five consecutive cycles (Figure 4 (A)). Few data points
353 with low flux after 60 minutes (start of second cycle) are due to the restart of system after cleaning
354 step, where there was a short lag until system reached the maximum initial flux. Factors
355 influencing these data points are established vacuum in the flask and tubing in addition to length
356 of the tubing. Air scour improved the fouling behavior in the TFNC-CNF membrane compared
357 with the system in stage 1. In specific, the TFNC-CNF membrane underwent flux decline (62.3 to
358 36.7 LMH for first hour) in comparison to condition without air scouring (46.4 to 26.2 LMH),
359 while the flux was constantly higher in the system with air scouring throughout the experiment.
360 The PVDF membrane flux changed from 30.4 LMH to 21.2 LMH with air scouring and declined
361 from 21.3 to 13.2 when air scouring was not applied (stage 1). Likewise, the flux of the PVDF
362 membrane was constantly higher in the air scoured system compared to system without air scour
363 suggesting that air scouring lightened fouling for both membranes. At the end of the experiment
364 (5 filtration cycles, 300 min), 8.4 L of permeate was collected in the TFNC-CNF membrane, which
365 was 1.7 times of the permeate volume (5.0 L) collected in the PVDF membrane (Figure 4(B)).
366 TOC, TP, and TC concentrations in the MLSS suspension (3090 ± 325 mg/L) and in the
367 permeate was characterized at stage 3, with air scouring. The TOC in MLSS represents the foulants
368 in bulk suspension and TOC rejection rate was calculated to present the foulants rejection in the

lab scale sMBR system. For both TFNC-CNF and PVDF membranes, TOC increased with time (Figure S5). For the TFNC-CNF membrane, the rejection rate was consistently above 83.2% (started at 83.2% and reached 92.2% at t = 120 and 96% at t = 300 min, respectively). In contrast, the PVDF membrane exhibited low TOC rejection during the first hour (started at 13.3% and increased to 69.8%) and the rejection rate continuously increased to 89.2%% by the end of the experiment. Proteins and polysaccharides are the major components in SMP and EPS, contributing to biofouling and their contribution were determined by characterizing TP and TC in SMP and extracted EPS samples. The TP rejection rate for the TFNC-CNF membrane was 56% while for the PVDF membrane it was half this value (27.2%). In addition, TC rejection by the TFNC-CNF membrane was 71.3% and slightly lower than the TC retention by the PVDF membrane (82.6%).

3.4 Membrane Surface Characteristics before and after Filtration

The surface morphology of the pristine and fouled TFNC-CNF and PVDF membranes was examined using SEM. The SEM images (Figures 5 (a) and (d)) clearly showed the surface of electrospun PAN substrate was covered by a thin layer of CNF. In Figure 5 panels (d) and (f), the CNF barrier layer was influenced by the high energy electron beam as the TFNC-CNF membrane would bend under this condition. The cross-section image of the pristine membrane (Figure 5 (d)) illustrates the thickness of the CNF barrier layer in TFNC-CNF membrane was 115 nm. SEM images illustrate the morphology changes on the surface of TFNC-CNF and PVDF membranes before and after washing at both test conditions (MLSS and supernatant filtration). For example, Figure 5 (b) shows the surface morphology of the TFNC-CNF and PVDF membranes employed for MLSS filtration at the end of the fourth cycle. The cross section view of the membranes showed a thinner cake layer on the surface of the TFNC-CNF membrane compared to the PVDF membrane

(~204.2 vs. ~516 nm), suggesting accumulation of more foulants on the surface of the PVDF membrane (Figure 5 (e)). The surface topography of the membranes used for supernatant filtration after fouling and subsequent washing indicated significantly less cells on the TFNC-CNF membrane (Figure 5 (c)), which was also confirmed in the cross section view (Figure 5 (f)). However, on the surface of the PVDF membrane, the presence of bacterial cells was observed, and the thickness of the cake layer was measured to be 671.3 nm. In Figure 5 (c), the fiber-like structure underneath the CNF layer is the electrospun PAN. The PAN support has high porosity (80%) and a mean pore size of 400-600 nm. The absence of a cake layer on surface of the TFNC-CNF membrane can explain the overall higher flux of this membrane during supernatant filtration in comparison to MLSS filtration.

Contact angle analysis showed the initial angle of the pristine TFNC-CNF membrane was 30.6°. After 10 seconds, a 52% reduction in the contact angle was observed. The contact angle was near zero in less than 30 seconds, suggesting the high hydrophilicity of the pristine TFNC-CNF membrane (Table 1). In contrast, the initial contact angle of the pristine PVDF membrane was 72° ± 0.25° and remained approximately unchanged over 30 seconds, indicating the relative hydrophobicity of this membrane. For both MLSS and supernatant filtration tests, the TFNC-CNF membrane became more hydrophobic after being used due to adsorption of foulants on the surface which is confirmed in Table 1. In addition, Figure S4 shows the ζ- potential of the pristine TFNC-CNF membrane had greater negative surface charge compared with the PVDF membrane over the pH range tested.

The surface functional groups of the sludge, sludge supernatant, as well as the surface of the pristine and the used and washed membrane was analyzed by ATR-FTIR spectroscopy to further explore the interactions of membranes with MLSS and supernatant, as shown in Figure 6. The

spectra showed bands at 3346 cm^{-1}, 3283 cm^{-1} and 2900 cm^{-1} wavenumber and were attributed to O-H, N-H, and C=O stretching vibrations, respectively, on the TFNC-CNF membrane surface. The bands in 1700 to 1300 cm^{-1} region belong to amide I, II and III stretching vibrations. The peak at 1655 cm^{-1} is attributed to C=O stretching vibration of amide I, while, peaks at 1538 cm^{-1} and 1230 cm^{-1} pin on N-H deformation of amide II and C-N stretching vibration of amide III (Mallamace et al. 2015, Zhang et al. 2015, Zhou et al. 2007). These peaks were detected in all samples except for pristine membranes, which showed the presence of protein in MLSS and supernatant and those on the surface of the fouled membranes. FTIR spectra demonstrates the existence of polysaccharides in sludge sample and those on the surface of fouled TFNC-CNF and PVDF membranes (both used and washed), where the observed peaks represented the following motions: stretching vibrations of C-O and C-C at 1131 cm^{-1} and 1082 cm^{-1} and vibrations of C-O-C and C-O-H at 1041 cm^{-1} and 983 cm^{-1}, respectively.

4 Discussion

4.1 Membrane Fouling

The TFNC-CNF membrane possesses a hydrophilic and negatively charged surface, leading to strong electrostatic repulsion of proteins in the feed wastewater (van Reis and Zydney 2007). During the first stage of this study, ultrafiltration was conducted continuously until the permeation flux was nearly stable after 240 minutes. The flux dropped more abruptly during the first 30 minutes for both pressures and both membrane materials used. Sludge has high affinity for hydrophobic membranes; however, when an initial cake layer forms, the surface of TFNC-CNF membrane also becomes more hydrophobic and so that causes an increase in SMP and EPS affinity

to the membrane surface. The electrostatic repulsion between the negatively charged TFNC-CNF surface and negatively charged foulants diminishes the adhesion interaction between them, thus leading to a high flux recovery ratio after cleaning. As a result, the better performance of TFNC-CNF membrane is due to its surface characteristics with stronger electrostatic repulsive forces between the surface of the membranes and foulants in the system (Hadi et al. 2019). The greater hydrophilicity of the TFNC-CNF membrane compared with that of the PVDF membrane also facilitates higher initial flux. The flux of the TFNC-CNF membrane was in the range for aerobic MBRs used in practice and higher than those of anaerobic MBRs, which are in range of 5-12 LMH (He et al. 2005, Herrera-Robledo et al. 2010, Judd 2010, Smith et al. 2012).

4.2 Membrane Flux Change and Recovery

The flux recovery of the TFNC-CNF membrane for both MLSS and supernatant filtration was more than 80%. The general trend in the flux decline in case of MLSS and supernatant filtration was similar for both membranes. However, for supernatant filtration the higher initial and final fluxes were due to limited total solids (TS) (EPS removed by centrifugation); while in case of MLSS filtration bacterial flocs attached via EPS and coexist with SMP thereby contributing to greater fouling. In addition, taking the flux data and SEM images into consideration, together they suggest the irreversible fouling is mostly due to pore blockage.

The results from dead-end filtration experiments demonstrate that the hydrophilic/hydrophobic nature of both membranes after being used for MLSS/supernatant filtration varied compared with the pristine membranes (Table 1). The TFNC-CNF membrane became more hydrophobic when used and washed. However, the contact angle data indicates the TFNC-CNF membranes maintained relatively lower hydrophobic properties in comparison to the PVDF membrane. The

increase in contact angle for the TFNC-CNF membrane is due to the hydrophobicity of the sludge remaining on the surface. Figure S4 illustrates that the surface ζ- potential is pH dependent. Surface of both membranes were negatively charged and with increase in pH, ζ- potential was more negative. The higher net negative surface charge of the TFNC-CNF membrane at all pH values indicates its capability in repelling the negatively charged particles i.e. proteins (most proteins in EPS have isoelectric point of 5-6 and the conventional wastewater treatment processes work at or slightly above this range) in the wastewater (Zhang et al. 2015).

4.3 Membranes Performance with Air Scouring

In the final set of experiments, the use of air scouring in the submerged ultrafiltration system has showed improved performance for the PVDF membrane, i.e., a higher initial flux and overall higher flux during the first one hour of experiment and sequent continuous ~65% flux recovery after each wash cycle. However, the initial flux of each stage was very close to the final flux from the previous cycle (i.e., 19.9 *vs* 20 LMH at the start of 3rd cycle and end of 2nd cycle, where the final fluxes after all cycles were slightly different and continuously decreasing with time). The TFNC-CNF membrane exhibited higher flux values throughout the experiments with air scour and could recover the initial flux after cleaning steps. SEM images from stage 2 confirmed thinner cake layer formation with MLSS filtration that could explain why TFNC could not recover 100% its initial flux. The TFNC-CNF membrane accumulated 40% more filtrate volume at the end of the experiments, which could be explained by its high affinity for water (Fu et al. 2017, Gustafsson et al. 2017).

The foulants concentration in the feed and permeate showed rejection of total polysaccharides and total proteins for both the TFNC-CNF and PVDF membranes. The rejection rate of

polysaccharide was high for both membranes which is in agreement with the literature indicating polysaccharides possess large size and gelation behavior (at acidic and neutral pH values), which results in their retention and accumulation in the mixed liquor and cake layer formation more than protein and humic substances (Wang and Waite 2009). Furthermore, proteins have a lower tendency to bond with the TFNC-CNF membranes (Gustafsson et al. 2017), which might allow them to be more easily removed from the surface of these membranes. In addition, the results are in good agreement with this fouling removability as more protein rejection was observed for the TFNC-CNF membranes. Proteins are largely negatively charged at neutral pH. Therefore, the electrostatic repulsion between membrane and protein mainly contributes to the low attachment. Based on the ATR-FTIR spectra, the major foulants identified on the membranes are polysaccharide and proteins, which are major contributors to SMP and EPS (Zhou et al. 2007).

The rejection rate of TOC for the both membranes increased over time which could be explained by formation of the gel/cake layer serving as a secondary membrane, which agrees with literature on SMP impact on UF/NF and RO membranes (Ding et al. 2016, Jarusutthirak and Amy 2006). The presence of peaks related to vibrational absorption of polysaccharides and proteins in ATR-FTIR spectra of both sludge and fouled membranes were consistent in this study, showing the evidence of membrane fouling caused by protein and polysaccharide content of SMP and EPS. None of these peaks were present on the surface of pristine membranes.

4.4 Membrane Surface Characteristics

SEM images of the fouled membranes suggest the fouling could be attributed to pore blockage as well as the cake layer formation due to the deposition of sludge as a result of suction force and the shear force generated by the air scouring module. These results agree with the previous study

by Meng et al. (Meng et al. 2006). SEM images from dead-end cell filtration tests suggest sludge flocs have more affinity to the PVDF membranes, as there were signs of bacterial cells on the surface of the fouled PVDF membrane used in ultrafiltration. In contrast, for the TFNC-CNF membrane there was less evidence of cells. For example, on the samples from sludge supernatant filtration, there were no cells observed and visually the fouled TFNC-CNF membrane looked similar to the pristine TFNC-CNF membrane. The sludge layer thickness on top of the PVDF membrane was approximately 516.8 nm, while the cake layer on TFNC-CNF membrane was 204.2 nm (considering ~114.8 nm thickness of the nano-cellulose fibrous layer), which confirmed the reduced fouling behavior of the TFNC-CNF membrane. Generally, hydrophilic bacteria have a tendency to attach to the hydrophilic surface, where the same is also found for the hydrophobic microorganisms. The study by Chao et al showed that the majority of microorganisms in activated sludge exhibit medium hydrophobicity (i.e. Nitrospira), which can be used to explain the bacterial cells attachment to the surface of the PVDF (Chao et al. 2014). Considering the change of the contact angle for TFNC-CNF membrane, when it becomes more hydrophobic there is increasing chance of experiencing biofouling. Similar pattern was seen in samples from sludge supernatant filtration, where the PVDF membrane had a thicker cake layer formed but the TFNC-CNF membrane showed no evidence of cake layer. SEM images suggest the thicker bio-cake layer (>2X thickness) could be the reason for lower flux recovery for the PVDF membrane.

5 Conclusions

In this study, the anti-biofouling performance of the TFNC-CNF membrane has been studied and compared with the PVDF membrane in a short-term operation of MBR for MLSS and

supernatant collected for real wastewater ultrafiltration. The main conclusions of this study are as following:

- At low constant absolute transmembrane pressure, the TFNC-CNF membrane exhibited higher stabled flux in comparison to commercial PVDF membrane filtering MLSS.
- The cake layer formed on the surface of the TFNC-CNF membrane was effortlessly removed using water jet which can eliminate cost of chemical cleaning. Hence, the membrane could retrieve its initial flux.
- Both membranes demonstrated higher performance ultrafiltration of supernatant, suggesting placement of the membrane module in a subsequent tank following the bioreactor can improve filtration efficiency
- Upgrading the systems with air scouring alleviate biofouling and improves the performance of both membranes utilized in this study. The combination of constant water flow cleaning and air scouring had positive impact on membrane performance.

6. Acknowledgment

This work was supported by a grant to the Center for Clean Water Technology (CCWT) from the New York State Department of Environmental Conservation (NYS-DEC). BSH thanks the financial support from the Polymer Program of the Division of Materials Science in the National Science Foundation (DMR-1808690). The authors are also grateful for the assistance of Caitlin Asato, CCWT, Xiangyu Huang, Department of Chemistry, Alexander Chow and Alexandre Georges, Department of Civil Engineering, College of Engineering and Applied Sciences, Stony Brook University.

552 **References**

553 Abbassi, R., Yadav, A.K., Huang, S. and Jaffe, P.R. (2014) Laboratory study of nitrification,
554 denitrification and anammox processes in membrane bioreactors considering periodic aeration.
555 Journal of Environmental Management 142, 53-59.
556 Abegglen, C., Joss, A., McArdell, C.S., Fink, G., Schlusener, M.P., Ternes, T.A. and Siegrist, H.
557 (2009) The fate of selected micropollutants in a single-house MBR. Water Research 43(7),
558 2036-2046.
559 Abouzeid, R.E., Khiari, R., El-Wakil, N. and Dufresne, A. (2019) Current State and New Trends
560 in the Use of Cellulose Nanomaterials for Wastewater Treatment. Biomacromolecules 20(2),
561 573-597.
562 Arabi, S. and Nakhla, G. (2009) Characterization of foulants in conventional and simultaneous
563 nitrification and denitrification membrane bioreactors. Separation and Purification Technology
564 69(2), 153-160.
565 Bagchi, S., Biswas, R. and Nandy, T. (2012) Autotrophic Ammonia Removal Processes: Ecology
566 to Technology. Critical Reviews in Environmental Science and Technology 42(13), 1353-
567 1418.
568 Chao, Y., Guo, F., Fang, H.H. and Zhang, T. (2014) Hydrophobicity of diverse bacterial
569 populations in activated sludge and biofilm revealed by microbial adhesion to hydrocarbons
570 assay and high-throughput sequencing. Colloids Surf B Biointerfaces 114, 379-385.
571 de Oliveira, T.S., Corsino, S.F., Di Trapani, D., Torregrossa, M. and Viviani, G. (2018) Biological
572 minimization of excess sludge in a membrane bioreactor: Effect of plant configuration on
573 sludge production, nutrient removal efficiency and membrane fouling tendency. Bioresour
574 Technol 259, 146-155.

575 Ding, A., Liang, H., Li, G., Derlon, N., Szivak, I., Morgenroth, E. and Pronk, W. (2016) Impact
576 of aeration shear stress on permeate flux and fouling layer properties in a low pressure
577 membrane bioreactor for the treatment of grey water. Journal of Membrane Science 510, 382-
578 390.
579 Faccini, M., Borja, G., Boerrigter, M., Morillo Martín, D., Martìnez Crespiera, S., Vázquez-
580 Campos, S., Aubouy, L. and Amantia, D. (2015) Electrospun Carbon Nanofiber Membranes
581 for Filtration of Nanoparticles from Water. Journal of Nanomaterials 2015, 1-9.
582 Falahati-Marvast, H. and Karimi-Jashni, A. (2020) A new modified anoxic-anaerobic-membrane
583 bioreactor for treatment of real wastewater with a low carbon/nutrient ratio and high nitrate.
584 Journal of Water Process Engineering 33.
585 Fu, W., Hua, L. and Zhang, W. (2017) Experimental and Modeling Assessment of the Roles of
586 Hydrophobicity and Zeta Potential in Chemically Modified Poly(ether sulfone) Membrane
587 Fouling Kinetics. Industrial & Engineering Chemistry Research 56(30), 8580-8589.
588 Galiano, F., André Schmidt, S., Ye, X., Kumar, R., Mancuso, R., Curcio, E., Gabriele, B., Hoinkis,
589 J. and Figoli, A. (2018) UV-LED induced bicontinuous microemulsions polymerisation for
590 surface modification of commercial membranes – Enhancing the antifouling properties.
591 Separation and Purification Technology 194, 149-160.
592 Gustafsson, S., Manukyan, L. and Mihranyan, A. (2017) Protein-Nanocellulose Interactions in
593 Paper Filters for Advanced Separation Applications. Langmuir 33(19), 4729-4736.
594 Hadi, P., Yang, M.Y., Ma, H.Y., Huang, X.Y., Walker, H. and Hsiao, B.S. (2019) Biofouling-
595 resistant nanocellulose layer in hierarchical polymeric membranes: Synthesis, characterization
596 and performance. Journal of Membrane Science 579, 162-171.

He, Y., Xu, P., Li, C. and Zhang, B. (2005) High-concentration food wastewater treatment by an anaerobic membrane bioreactor. Water Research 39(17), 4110-4118.

Herrera-Robledo, M., Morgan-Sagastume, J.M. and Noyola, A. (2010) Biofouling and pollutant removal during long-term operation of an anaerobic membrane bioreactor treating municipal wastewater. Biofouling 26(1), 23-30.

Huang, Z., Ong, S.L. and Ng, H.Y. (2011) Submerged anaerobic membrane bioreactor for low-strength wastewater treatment: effect of HRT and SRT on treatment performance and membrane fouling. Water Research 45(2), 705-713.

Jarusutthirak, C. and Amy, G. (2006) Role of soluble microbial products (SMP) in membrane fouling and flux decline. Environmental Science & Technology 40(3), 969-974.

Ji, L. and Zhou, J. (2006) Influence of aeration on microbial polymers and membrane fouling in submerged membrane bioreactors. Journal of Membrane Science 276(1-2), 168-177.

Jin, L., Wang, Z., Zheng, S. and Mi, B. (2018) Polyamide-crosslinked graphene oxide membrane for forward osmosis. Journal of Membrane Science 545, 11-18.

Jin, R.C. and Zheng, P. (2009) Kinetics of nitrogen removal in high rate anammox upflow filter. Journal of Hazardous Materials 170(2-3), 652-656.

Judd, S. (2006) The MBR Book: Principles and Applications of Membrane Bioreactors for Water and Wastewater Treatment, Elsevier, Oxford.

Judd, S. (2010) The MBR book: principles and applications of membrane bioreactors for water and wastewater treatment, Elsevier.

Kraemer, J.T., Menniti, A.L., Erdal, Z.K., Constantine, T.A., Johnson, B.R., Daigger, G.T. and Crawford, G.V. (2012) A practitioner's perspective on the application and research needs of membrane bioreactors for municipal wastewater treatment. Bioresour Technol 122, 2-10.

620 Krzeminski, P., Leverette, L., Malamis, S. and Katsou, E. (2017) Membrane bioreactors – A
621 review on recent developments in energy reduction, fouling control, novel configurations,
622 LCA and market prospects. Journal of Membrane Science 527, 207-227.
623 Kunacheva, C. and Stuckey, D.C. (2014) Analytical methods for soluble microbial products (SMP)
624 and extracellular polymers (ECP) in wastewater treatment systems: a review. Water Research
625 61, 1-18.
626 Laspidou, C.S. and Rittmann, B.E. (2002) A unified theory for extracellular polymeric substances,
627 soluble microbial products, and active and inert biomass. Water Research 36(11), 2711-2720.
628 Le-Clech, P. (2010) Membrane bioreactors and their uses in wastewater treatments. Appl
629 Microbiol Biotechnol 88(6), 1253-1260.
630 Le-Clech, P., Chen, V. and Fane, T.A.G. (2006) Fouling in membrane bioreactors used in
631 wastewater treatment. Journal of Membrane Science 284(1-2), 17-53.
632 Liu, H. and Fang, H.H. (2002) Extraction of extracellular polymeric substances (EPS) of sludges.
633 J Biotechnol 95(3), 249-256.
634 Liu, L., Zhao, F., Liu, J. and Yang, F. (2013) Preparation of highly conductive cathodic membrane
635 with graphene (oxide)/PPy and the membrane antifouling property in filtrating yeast
636 suspensions in EMBR. Journal of Membrane Science 437, 99-107.
637 Liu, Z., An, X., Dong, C., Zheng, S., Mi, B. and Hu, Y. (2017) Modification of thin-film composite
638 polyamide membranes with 3D hyperbranched polyglycerol for simultaneous improvement in
639 their filtration performance and antifouling properties. Journal of Materials Chemistry A 5(44),
640 23190-23197.

641 Ma, H., Burger, C., Hsiao, B.S. and Chu, B. (2014) Fabrication and characterization of cellulose
642 nanofiber based thin-film nanofibrous composite membranes. Journal of Membrane Science
643 454, 272-282.
644 Mallamace, F., Corsaro, C., Mallamace, D., Vasi, S., Vasi, C. and Dugo, G. (2015) The role of
645 water in protein's behavior: The two dynamical crossovers studied by NMR and FTIR
646 techniques. Comput Struct Biotechnol J 13, 33-37.
647 Mao, X., Myavagh, P.H., Lotfikatouli, S., Hsiao, B.S. and Walker, H.W. (2020) Membrane
648 Bioreactors for Nitrogen Removal from Wastewater: A Review. Journal of Environmental
649 Engineering 146(5).
650 Masuko, T., Minami, A., Iwasaki, N., Majima, T., Nishimura, S.-I. and Lee, Y.C. (2005)
651 Carbohydrate analysis by a phenol–sulfuric acid method in microplate format. Analytical
652 biochemistry 339(1), 69-72.
653 Meng, F., Chae, S.R., Drews, A., Kraume, M., Shin, H.S. and Yang, F. (2009) Recent advances in
654 membrane bioreactors (MBRs): membrane fouling and membrane material. Water Research
655 43(6), 1489-1512.
656 Meng, F., Yang, F., Xiao, J., Zhang, H. and Gong, Z. (2006) A new insight into membrane fouling
657 mechanism during membrane filtration of bulking and normal sludge suspension. Journal of
658 Membrane Science 285(1-2), 159-165.
659 Mutamim, N.S.A., Noor, Z.Z., Hassan, M.A.A., Yuniarto, A. and Olsson, G. (2013) Membrane
660 bioreactor: Applications and limitations in treating high strength industrial wastewater.
661 Chemical Engineering Journal 225, 109-119.
662 Peterson, G.L. (1977) A simplification of the protein assay method of Lowry et al. which is more
663 generally applicable. Analytical biochemistry 83(2), 346-356.

664 Rockström, J., Steffen, W., Noone, K., Persson, Å., Chapin III, F.S., Lambin, E.F., Lenton, T.M.,
665 Scheffer, M., Folke, C. and Schellnhuber, H.J. (2009) A safe operating space for humanity.
666 nature 461(7263), 472.
667 Shi, Y., Huang, J., Zeng, G., Gu, Y., Hu, Y., Tang, B., Zhou, J., Yang, Y. and Shi, L. (2017)
668 Evaluation of soluble microbial products (SMP) on membrane fouling in membrane
669 bioreactors (MBRs) at the fractional and overall level: a review. Reviews in Environmental
670 Science and Bio/Technology 17(1), 71-85.
671 Smith, A.L., Stadler, L.B., Love, N.G., Skerlos, S.J. and Raskin, L. (2012) Perspectives on
672 anaerobic membrane bioreactor treatment of domestic wastewater: a critical review.
673 Bioresource Technology 122, 149-159.
674 Su, Y.-C., Huang, C., Pan, J.R., Hsieh, W.-P. and Chu, M.-C. (2012) Fouling Mitigation by TiO2
675 Composite Membrane in Membrane Bioreactors. Journal of Environmental Engineering
676 138(3), 344-350.
677 Subtil, E.L., Silva, M.V., Lotto, B.A., Moretto, M.R.D. and Mierzwa, J.C. (2019) Pilot-scale
678 investigation on the feasibility of simultaneous nitrification and denitrification (SND) in a
679 continuous flow single-stage membrane bioreactor. Journal of Water Process Engineering 32.
680 van Reis, R. and Zydney, A. (2007) Bioprocess membrane technology. Journal of Membrane
681 Science 297(1-2), 16-50.
682 Wang, X.-m. and Waite, T.D. (2009) Role of gelling soluble and colloidal microbial products in
683 membrane fouling. Environmental Science & Technology 43(24), 9341-9347.
684 Yang, B., Chen, G. and Chen, G. (2012) Submerged membrane bioreactor in treatment of
685 simulated restaurant wastewater. Separation and Purification Technology 88, 184-190.

686 Yang, S., Yang, F.L., Fu, Z.M. and Lei, R.B. (2009) Comparison between a moving bed membrane
687 bioreactor and a conventional membrane bioreactor on organic carbon and nitrogen removal.
688 Bioresource Technology 100(8), 2369-2374.
689 Zhang, P., Shen, Y., Guo, J.S., Li, C., Wang, H., Chen, Y.P., Yan, P., Yang, J.X. and Fang, F.
690 (2015) Extracellular protein analysis of activated sludge and their functions in wastewater
691 treatment plant by shotgun proteomics. Sci Rep 5, 12041.
692 Zhou, J., Yang, F.-l., Meng, F.-g., An, P. and Wang, D. (2007) Comparison of membrane fouling
693 during short-term filtration of aerobic granular sludge and activated sludge. Journal of
694 Environmental Sciences 19(11), 1281-1286.
695

Graphical Abstract

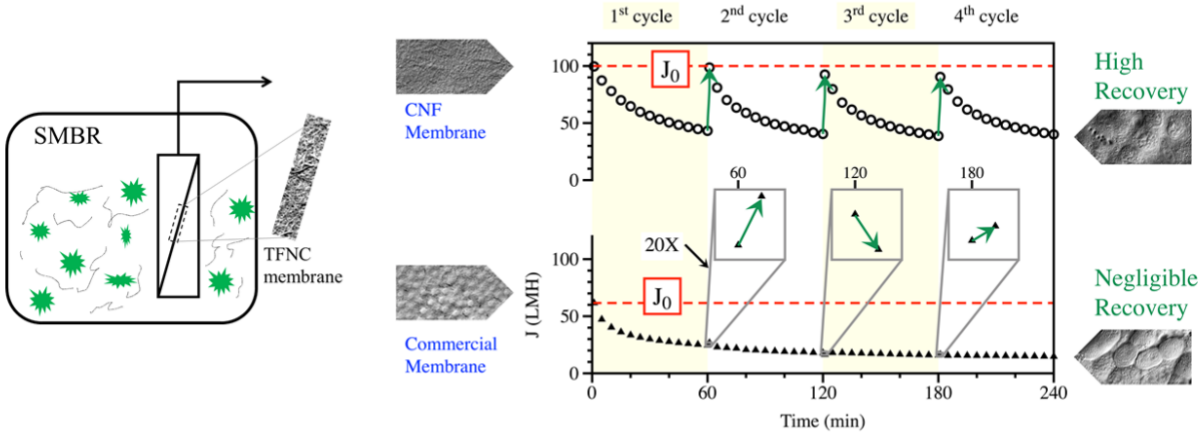

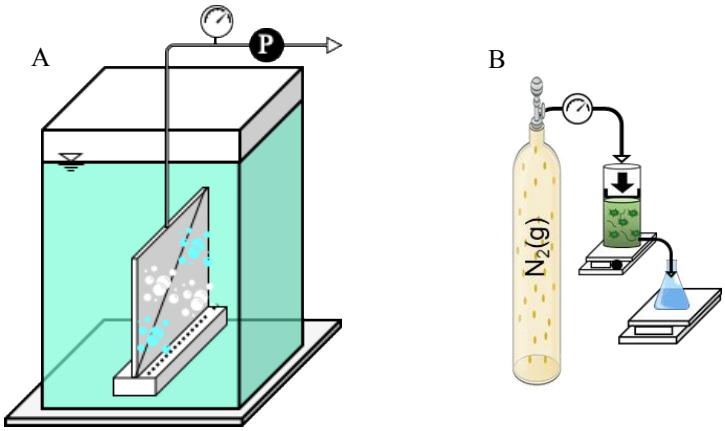

Figure 1. Schematic diagrams of (A) the submerged membrane filtration unit w/wo air scouring unit, and (B) the Sterlitech dead-end filtration cell for MLSS and supernatant filtration.

A

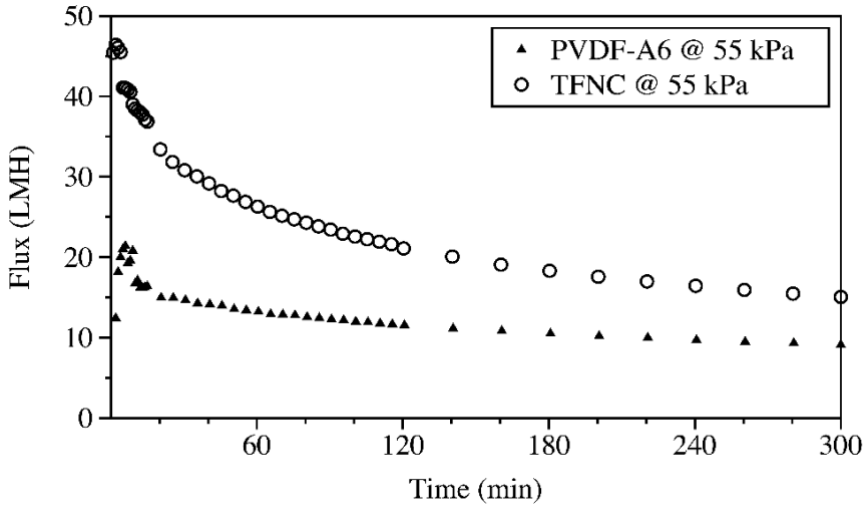

B

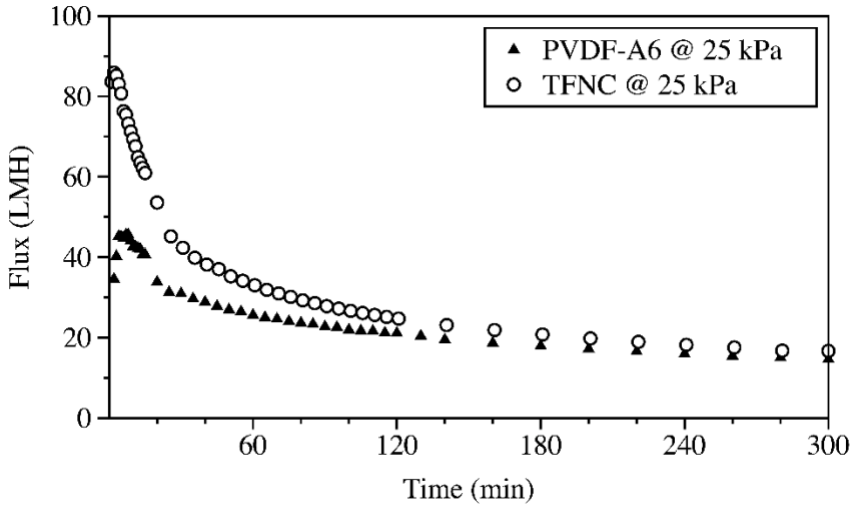

Figure 2. Flux change in TFNC-CNF coated membrane and PVDF-A6 membranes when filtering MLSS (2950 ± 50 mg/L) at (A) TMP_{abs}55 kPa and (B) TMP_{abs} 25 kPa.

A

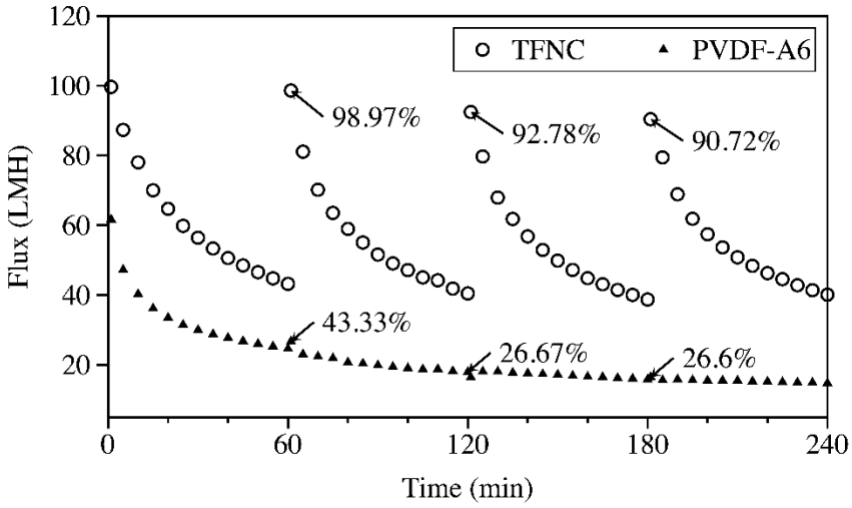

B

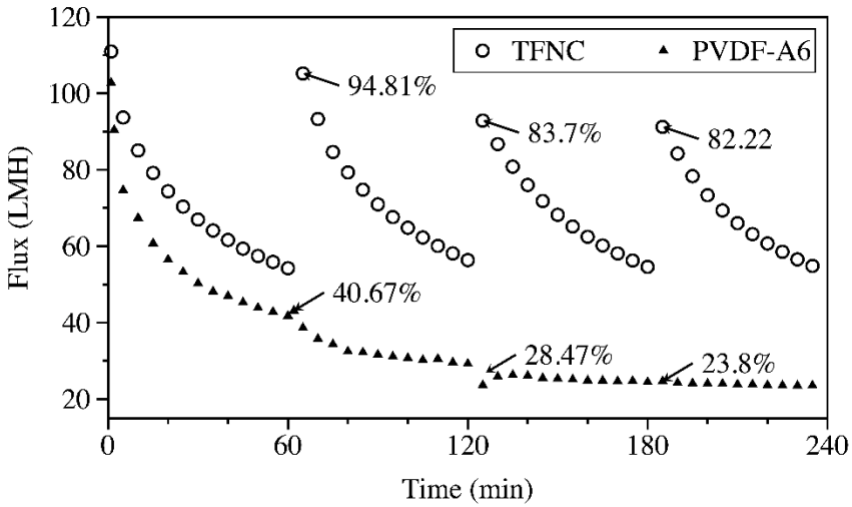

Figure 3. Flux change and recovery of TFNC-CNF coated membrane and PVDF-A6 membrane when filtering (A) MLSS (3000 ± 75mg/L); and (B) sludge supernatant at 55 kPa absolute pressure.

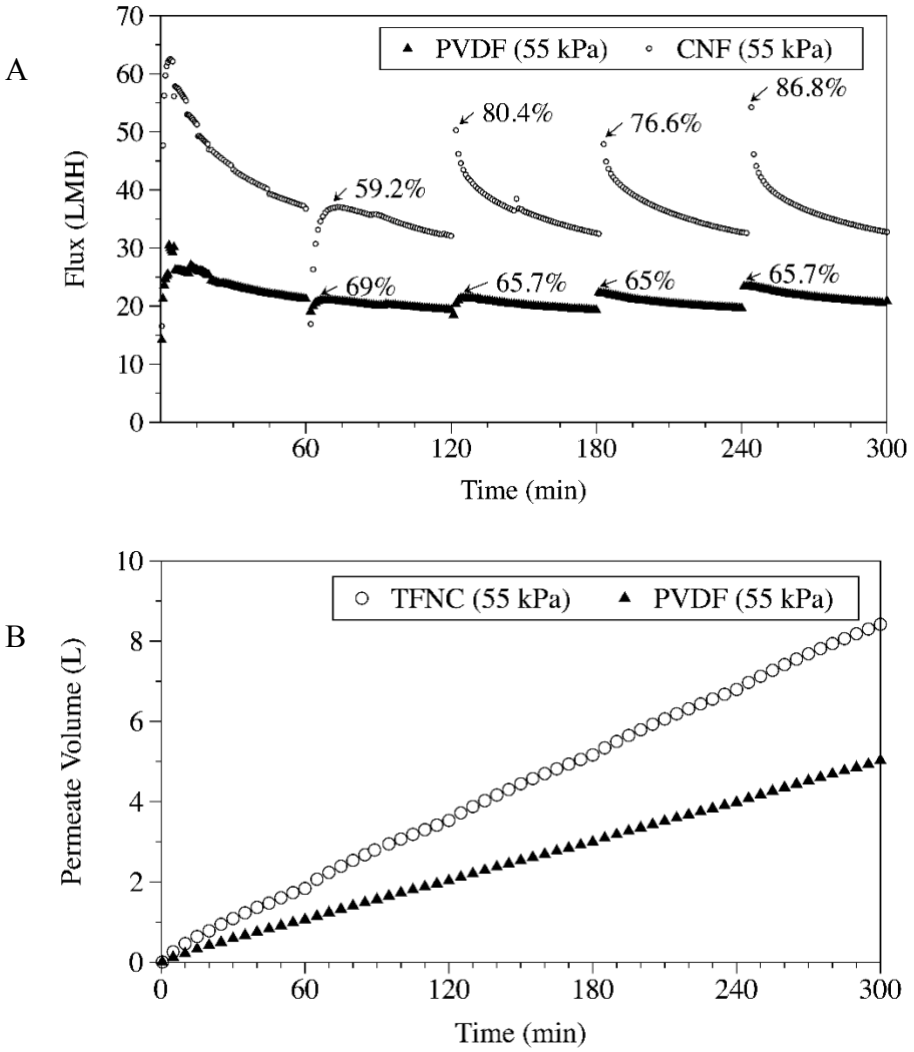

Figure 4. (A) Flux recovery and the (B) accumulative permeate volume of the TFNC-CNF coated membrane and PVDF membrane for MLSS filtration with air scouring.

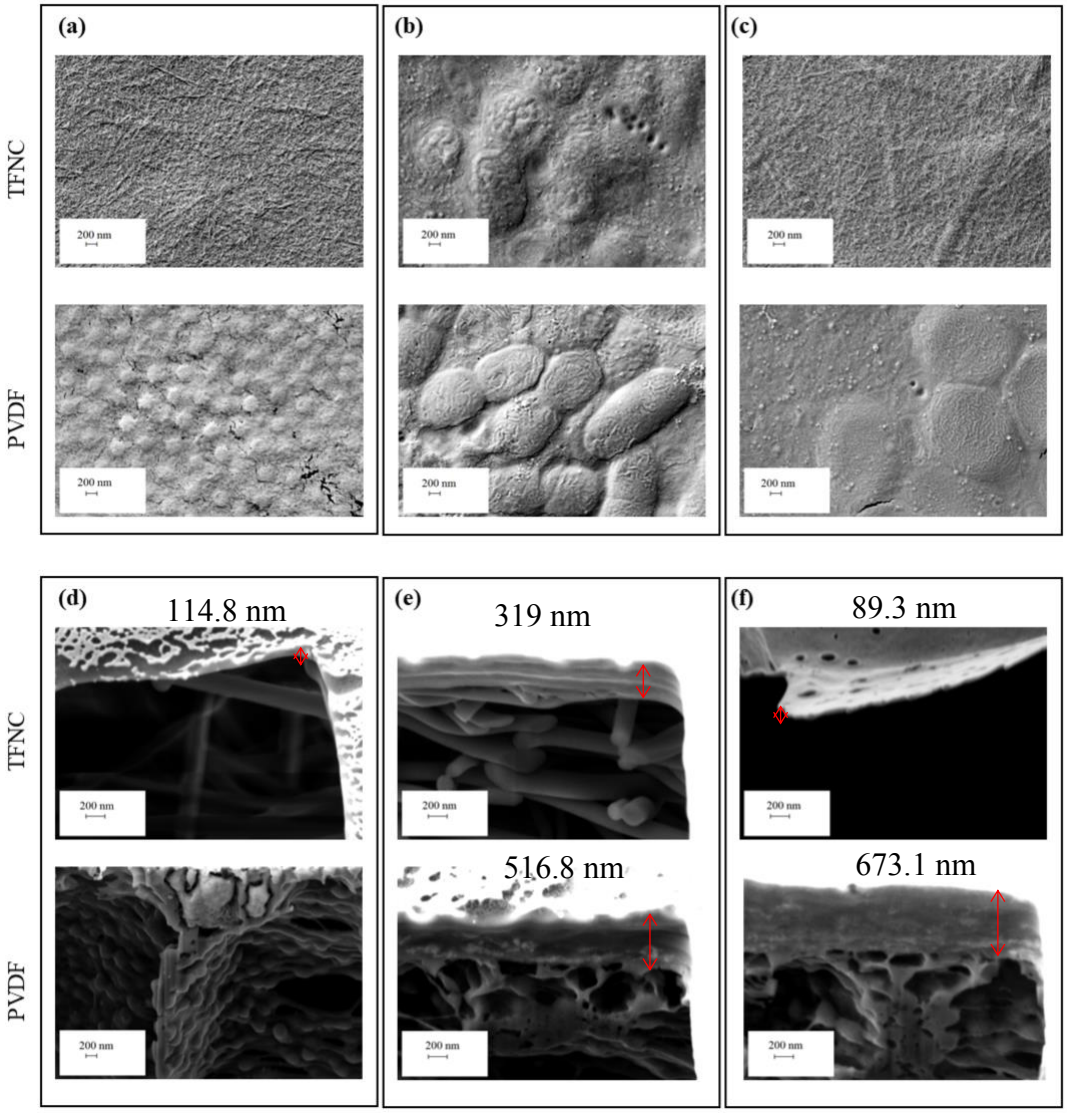

Figure 5. SEM images of the surface morphology and the cross-sectional views of TFNC and PVDF membranes at following conditions (a) & (d) pristine membrane, (b) & (e) washed membranes after 4 filtration cycles of MLSS, (c) & (f) washed membranes after 4 filtration cycles of sludge supernatant.

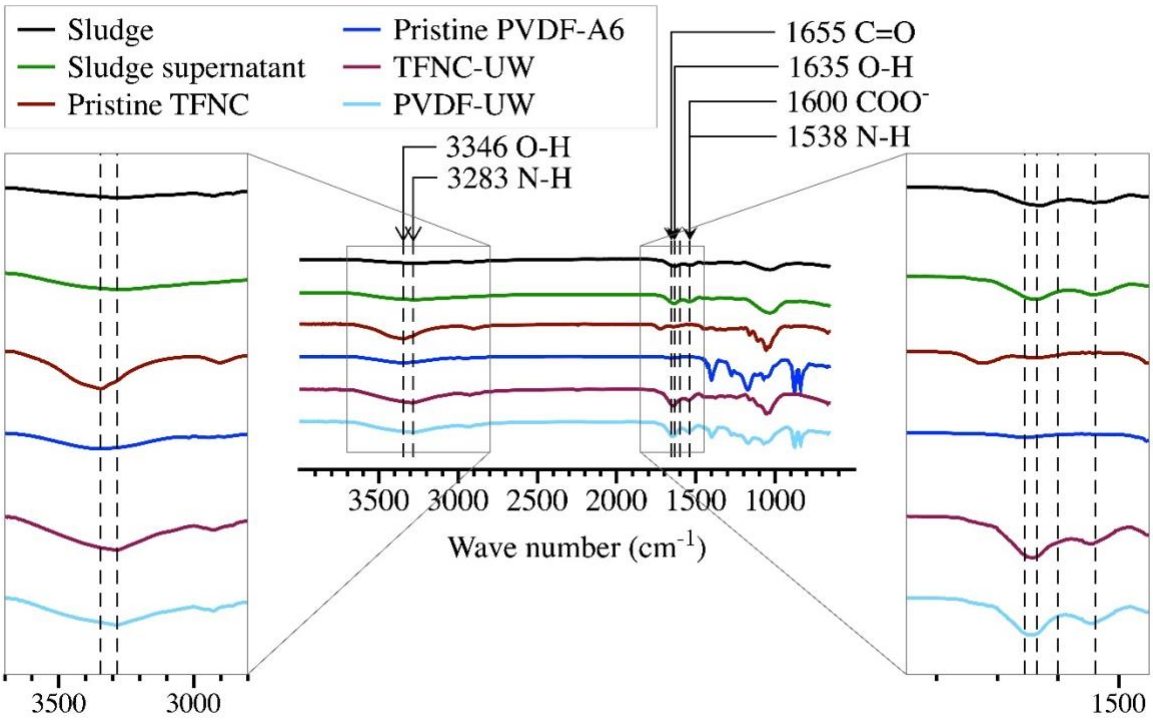

47

48 Figure 6. ATR-FTIR results for PVDF-A6 and TFNC-CNF coated membranes (pristine and UW:

49 used and washed)

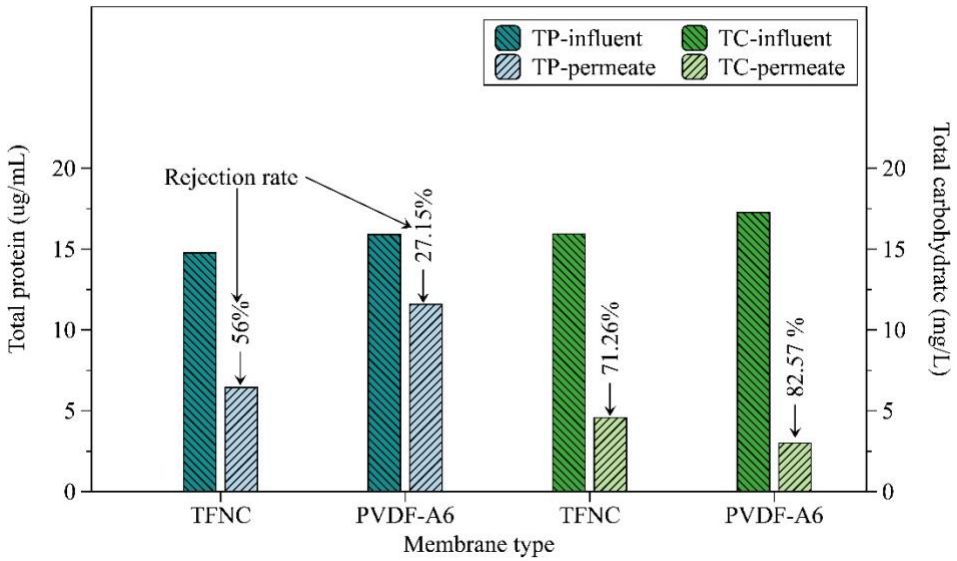

50

51 Figure 7. Total protein and total carbohydrate concentrations in influent and permeate samples

52

Table 1. Contact angle analysis of pristine membranes and membranes after filtration[1]

Time (s)	0		5		10		15		30	
PVDF-Pristine	72.0		72.3		72.3		72.2		71.7	
CNF-Pristine	30.6		17.0		14.7		12.9		~0	
PVDF-UW[2]	83.8		83.7		83.6		83.2		82.8	
CNF-UW	71.5		65.4		60.2		53.9		36.8	
PVDF-UW-S[3]	89.3		88.3		87.7		87.5		86.8	
CNF-UW-S	69.8		52.9		48.7		46.2		38.6	

[1]the used and washed membrane samples were taken at the end of the 4th filtration cycle at stage 2.
[2] UW: Used and washed membrane for MLSS filtration.
[3] UW-S: Used and washed membrane for sludge supernatant filtration.

57 Table 2. Comparison on different membrane filtration systems

Sample type	Configuration	Material	Pore size	Scale (L)	TMP (kPa)	Flux (LMH)	Area (m2)	Nitrification	Ref.
Real WW[1]	Submerged MBR+AS[2] Flat sheet	TFNC-CNF based & PVDF	50 nm	40	55 & 25	-	0.05	-	This study
Synthetic greywater	Submerged+AS Flat sheet	PES[3]	15 nm	60	5	-	0.06	-	(Ding et al. 2016)
Synthetic WW	Submerged Flat sheet	PS[4]	80 nm	20	25	600	-	99.2±0.5%	(Lu et al. 2016)
Real WW	Submerged HF[5]	-	40 nm	12.5 m^3	-	29 (max)	40	-	(Ferrero et al. 2011)
Food wastewater	Flat sheet	PES	-	-	200	13.1-18.9	0.32	-	(He et al. 2005)
BSA[6], SA[7] & HA[8]	Dead-end cell Flat sheet	TFC-PVDF	-	-	210		0.00041	-	(Asatekin et al. 2006)
Concentrated WW	Submerged AnMBR[9] Flat sheeet	PVDF	20-70 kDa	6.5	<30 kPa	1.8	0.03	-	(Lin et al. 2009)
Real WW	AnMBR Tubular	-	40 kDa		355	14.5 & 17.1	0.0081		(Herrera-Robledo et al. 2010)
Real WW	MBBR[10] & CMBR[11] +AS HF Submerged	PP[12]	0.1 µm	10& 30	-	4.17 & 6.25	0.2 & 0.4	-	(Yang et al. 2009)
Real WW	Dead-end cell UF/NF/RO	PA[13]	-	10 L	344 & 480	35	-	-	(Jarusutthirak and Amy 2006)

[1] Wastewater
[2] Air scouring
[3] Polyethersulfone
[4] Polysulfone
[5] Hollow fiber
[6] Bovine serum albumine
[7] Sodium alginate
[8] Humic acid
[9] Anaerobic MBR
[10] Moving bed biofim MBR
[11] Conventional MBR
[12] Polypropyene
[13] Plyamide

Synthetic WW	SBMBR[14] HF	PP	0.1 µm	3.5	9.81	20 & 40	0.1	-	(Zhou et al. 2007)
Synthetic WW	SBMBR+AS Flat sheet	PP	0.1 µm	10	-	-	0.4	>89%	(Dong and Jiang 2009)
Grey water	MBBMBR[8] HF	HDPE	0.2 µm	200		12.9	6	-	(Jabornig and Favero 2013)

Asatekin, A., Menniti, A., Kang, S., Elimelech, M., Morgenroth, E. and Mayes, A.M. (2006) Antifouling nanofiltration membranes for membrane bioreactors from self-assembling graft copolymers. Journal of Membrane Science 285(1-2), 81-89.

Ding, A., Liang, H., Li, G., Derlon, N., Szivak, I., Morgenroth, E. and Pronk, W. (2016) Impact of aeration shear stress on permeate flux and fouling layer properties in a low pressure membrane bioreactor for the treatment of grey water. Journal of Membrane Science 510, 382-390.

Dong, B. and Jiang, S. (2009) Characteristics and behaviors of soluble microbial products in sequencing batch membrane bioreactors at various sludge retention times. Desalination 243(1-3), 240-250.

Ferrero, G., Monclus, H., Sancho, L., Garrido, J.M., Comas, J. and Rodriguez-Roda, I. (2011) A knowledge-based control system for air-scour optimisation in membrane bioreactors. Water Science and Technology 63(9), 2025-2031.

He, Y., Xu, P., Li, C. and Zhang, B. (2005) High-concentration food wastewater treatment by an anaerobic membrane bioreactor. Water Research 39(17), 4110-4118.

Herrera-Robledo, M., Morgan-Sagastume, J.M. and Noyola, A. (2010) Biofouling and pollutant removal during long-term operation of an anaerobic membrane bioreactor treating municipal wastewater. Biofouling 26(1), 23-30.

Jabornig, S. and Favero, E. (2013) Single household greywater treatment with a moving bed biofilm membrane reactor (MBBMR). Journal of Membrane Science 446, 277-285.

Jarusutthirak, C. and Amy, G. (2006) Role of soluble microbial products (SMP) in membrane fouling and flux decline. Environmental Science & Technology 40(3), 969-974.

Lin, H.J., Xie, K., Mahendran, B., Bagley, D.M., Leung, K.T., Liss, S.N. and Liao, B.Q. (2009) Sludge properties and their effects on membrane fouling in submerged anaerobic membrane bioreactors (SAnMBRs). Water Research 43(15), 3827-3837.

Lu, H., Xue, Z., Saikaly, P., Nunes, S.P., Bluver, T.R. and Liu, W.T. (2016) Membrane biofouling in a wastewater nitrification reactor: Microbial succession from autotrophic colonization to heterotrophic domination. Water Research 88, 337-345.

Yang, S., Yang, F.L., Fu, Z.M. and Lei, R.B. (2009) Comparison between a moving bed membrane bioreactor and a conventional membrane bioreactor on organic carbon and nitrogen removal. Bioresource Technology 100(8), 2369-2374.

Zhou, J., Yang, F.-l., Meng, F.-g., An, P. and Wang, D. (2007) Comparison of membrane fouling during short-term filtration of aerobic granular sludge and activated sludge. Journal of Environmental Sciences 19(11), 1281-1286.

[14] Sequencing batch MBR

Supporting Information

Enhanced anti-fouling performance in MBRs using cellulose nanofiber coated membrane

Sarah Lotfikatouli[a], Pejman Hadi[b], Mengying Yang[b], Harold Walker[c], Benjamin S. Hsiao[b], Christopher Gobler[d, e], Michael Reichel[f], Xinwei Mao[a,*]

[a] Department of Civil Engineering, College of Engineering and Applied Sciences, Stony Brook University, Stony Brook, NY 11794

[b] Department of Chemistry, Stony Brook University, Stony Brook, NY 11794

[c] Department of Civil and Environmental Engineering, Worcester Polytechnic Institute, Worcester, MA 01609

[d] New York State Center for Clean Water Technology, Stony Brook University, Stony Brook, NY 11794

[e] School of Marine and Atmospheric Sciences, Stony Brook University, Stony Brook, NY 11794

[f] Town of Riverhead Sewer District, Riverhead, NY 11901

*Corresponding author: Xinwei Mao

Address: 2429 Computer Science Building, Stony Brook University, Stony Brook, NY11794

e-mail: xinwei.mao@stonybrook.edu

Supporting Information containing 6 pages, 5 figures and 1 table to accompany manuscript entitled.

TABLE OF CONTENT

SUPPORTING FIGURES

Supporting Figures

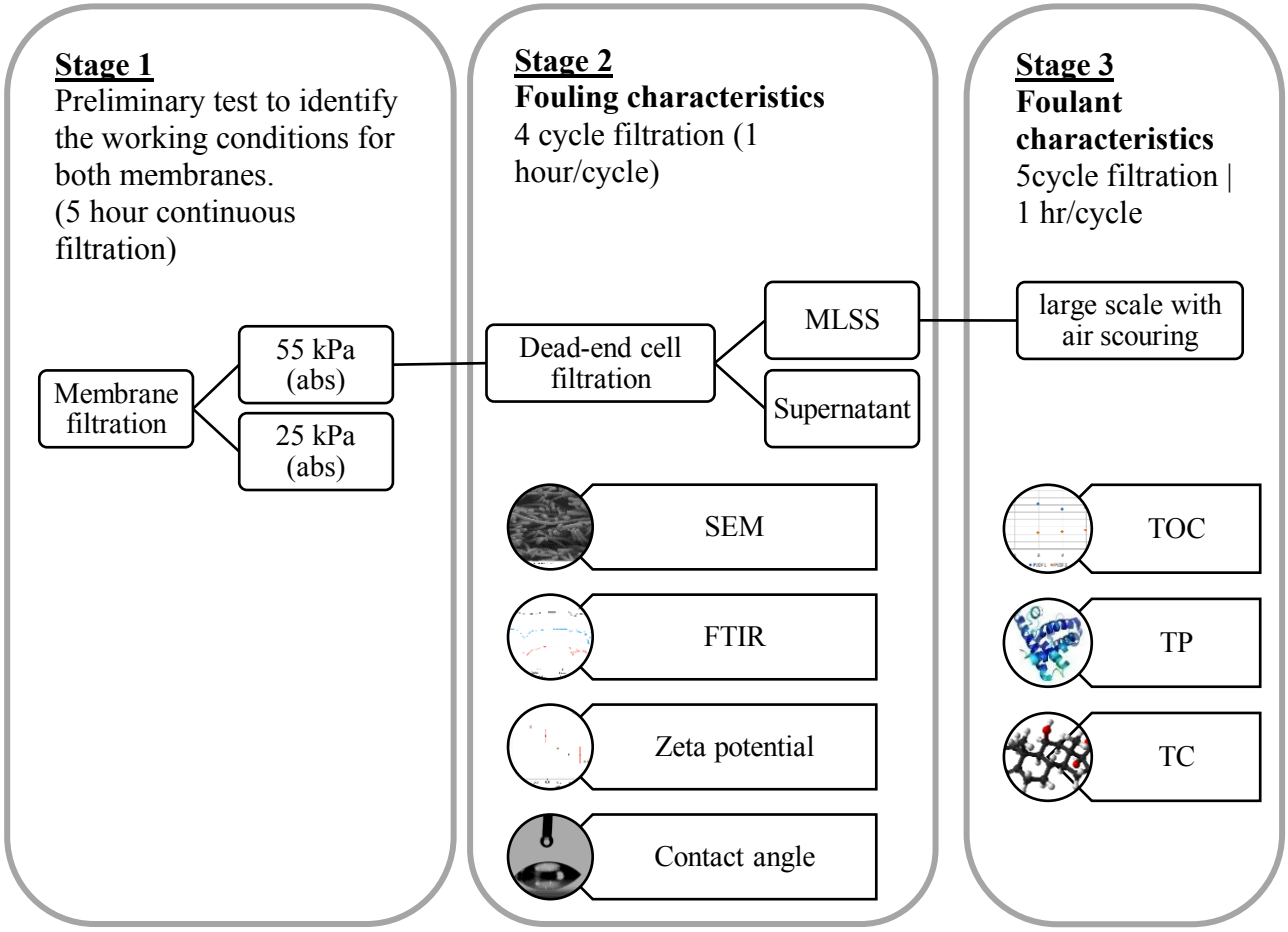

Figure S1. The overall workflow of the experiment in three stages.

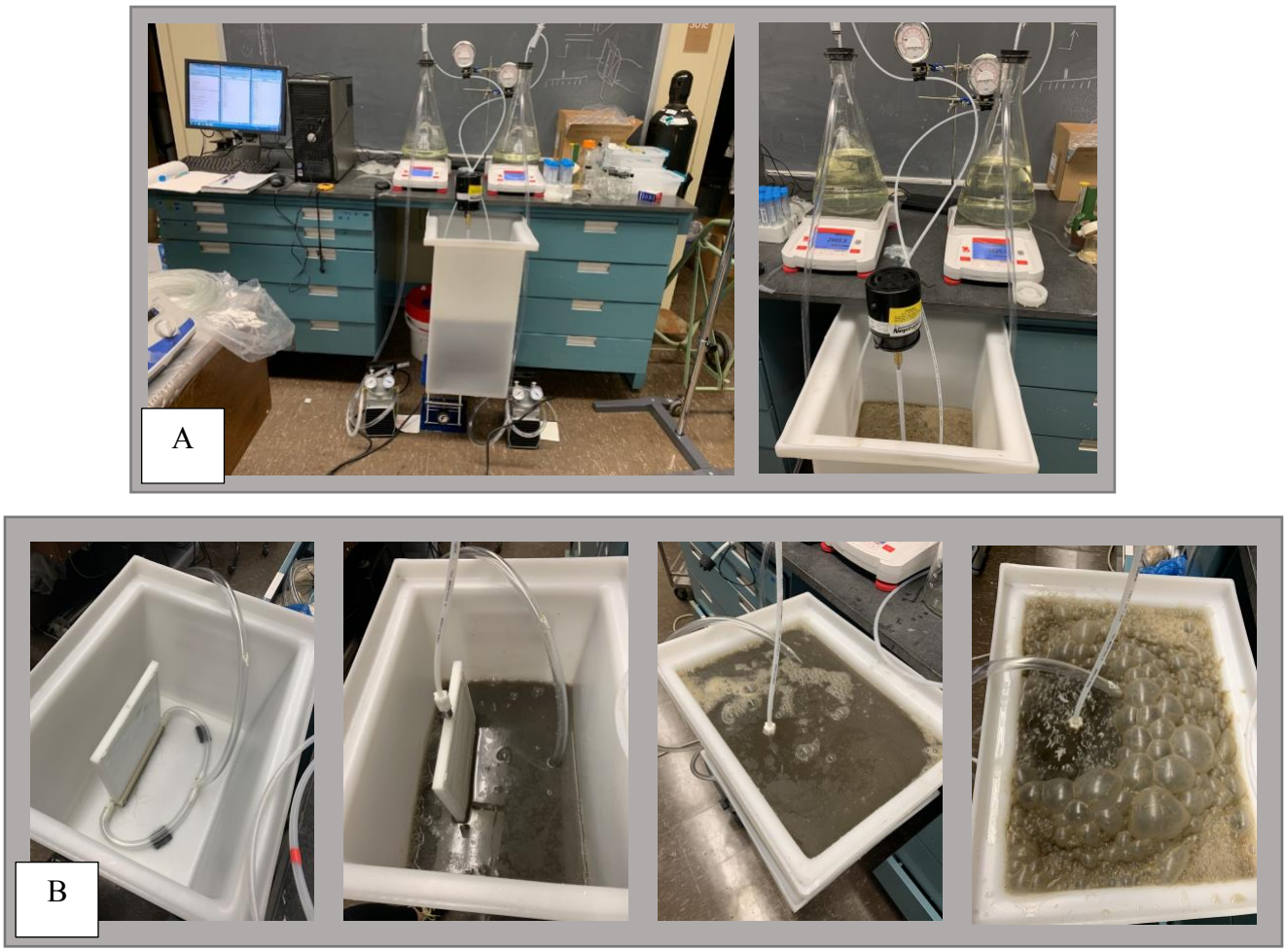

Figure S2. Overall system in (A) stage 2 and (B) stage 3.

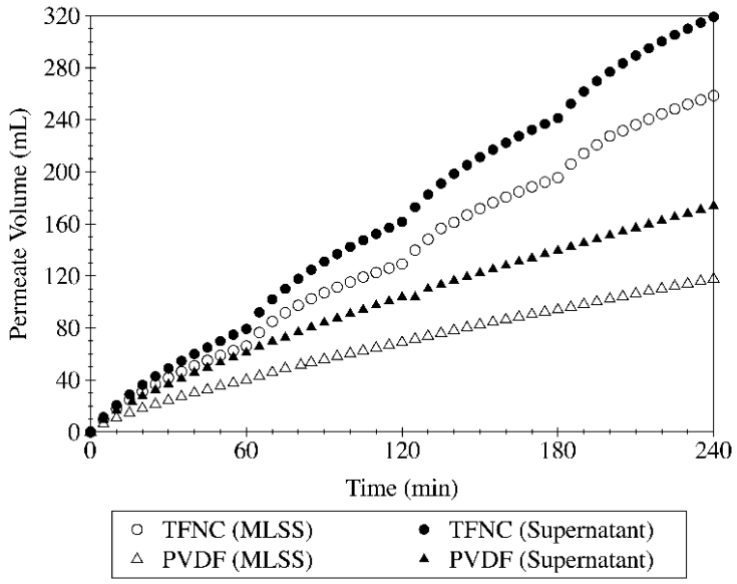

Figure S3. Accumulative permeate volume for TFNC-CNF coated and PVDF membranes for MLSS and supernatant filtration in stage 2.

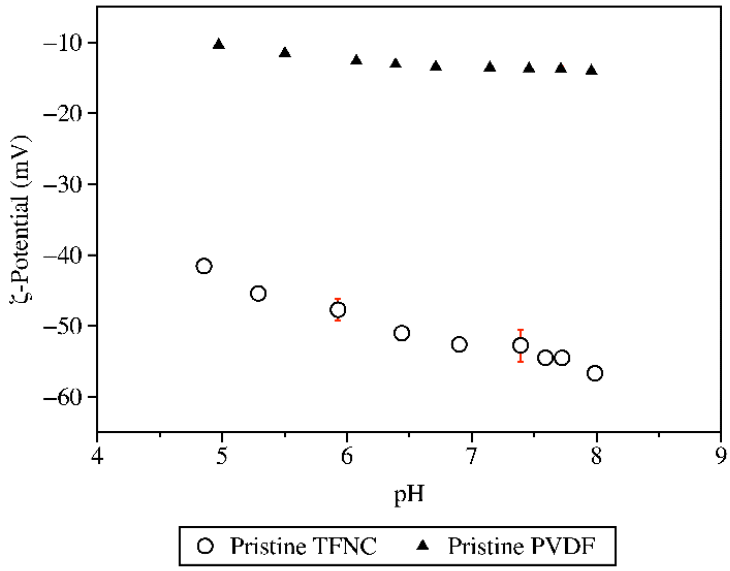

Figure S4. ζ- potential of pristine TFNC membrane and PVDF membrane.

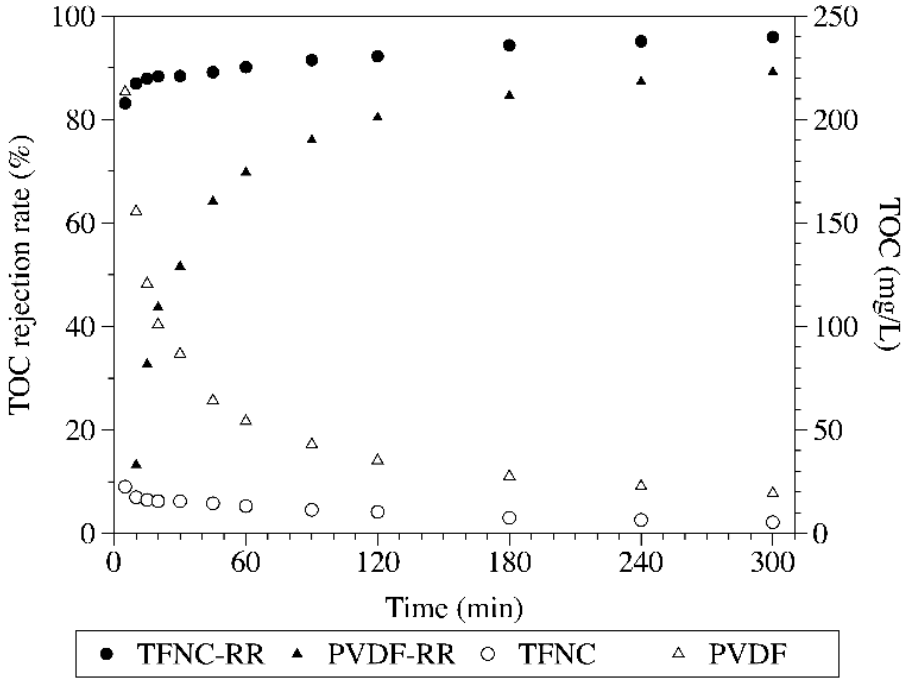

Figure S5. TOC rejection rate by TFNC and PVDF membranes (data points labeled with RR, left vertical axis) and TOC concentration in the permeate over time for TFNC and PVDF membranes (open circles).

Nominal Pore Size Analysis

Polystyrene microspheres with nominal sizes of 0.1 and 0.05 μm were used to determine the pore size of the TFNC and PVDF membranes for pristine and used membranes (after mixed liquor filtration). Total organic carbon (TOC) in influent sample and permeate was used to calculate TOC rejection rate based on stock solution concentration. The TOC rejection rate for pristine TFNC and PVDF membranes for were 96.4% and 95.4% for 0.05 μm polystyrene microspheres, and the rejection rate were 96% and 97% for 0.1 μm polystyrene microspheres demonstrating nominal pore size of smaller than 50 nm for both membranes. The TOC rejection rate increased by 1% for all used and washed membranes for both microsphere sizes.

Supporting Table

Table S1. Membrane fouling tests in different stages.

Stage	Membrane filtration unit	Reactor volume(L)	Filtration cycle (min)	Number of cycles	Physical cleaning	Membrane effective surface area (m^2)	Operational absolute pressures (kPa)
I	Submerged membrane filtration	40	300	1	N	0.05	55 25
II	Sterlitech Dead-end cell	0.25	60	4	Y	0.0015	55
III	Submerged membrane filtration with air scouring	40	60	5	Y	0.05	55